Title: Testing Gravity Using Type Ia Supernovae Discovered by Next Generation Wide Field Imaging Survey

Thematic Science Area: Cosmology and Fundamental Physics

Authors: and a list of authors

Lead Author Contact Information: Alex Kim; Physics Division, Lawrence Berkeley National Laboratory, 1 Cyclotron Road, Berkeley, CA, 94720; 1-510-486-4621; agkim@lbl.gov

Draft version January 24, 2019
Typeset using LaTeX default style in AASTeX62

Testing Gravity Using Type Ia Supernovae Discovered by Next Generation Wide Field Imaging Surveys

A. G. Kim,[1] G. Aldering,[1] P. Antilogus,[2] S. BenZvi,[3] S. Gontcho A Gontcho,[3] R. Graziani,[4] C. Harper,[1] C. Howlett,[5] D. Huterer,[6] C. Ju,[1] P.-F. Leget,[2] E. V. Linder,[1] P. McDonald,[1] J. Nordin,[7] S. Perlmutter,[1,8] N. Regnault,[2] M. Rigault,[9] and others

[1] *Physics Division, Lawrence Berkeley National Laboratory, 1 Cyclotron Road, Berkeley, CA, 94720*
[2] *Laboratoire de Physique Nucléaire et de Hautes Energies, Sorbonne Université, CNRS-IN2P3, 4 Place Jussieu, 75005 Paris, France*
[3] *Department of Physics and Astronomy, University of Rochester, Rochester, NY 14627, USA*
[4] *Université Clermont Auvergne, CNRS/IN2P3, Laboratoire de Physique de Clermont, F-63000 Clermont-Ferrand, France*
[5] *International Centre for Radio Astronomy Research, The University of Western Australia, Crawley, WA 6009, Australia*
[6] *Department of Physics, University of Michigan, 450 Church Street, Ann Arbor, MI 48109, USA*
[7] *Institut fur Physik, Humboldt-Universitat zu Berlin, Newtonstr. 15, 12489 Berlin, Germany*
[8] *Department of Physics, University of California Berkeley, 366 LeConte Hall MC 7300, Berkeley, CA, 94720-7300*
[9] *Université de Lyon, F-69622, Lyon, France; Université de Lyon 1, Villeurbanne; CNRS/IN2P3, Institut de Physique Nuclaire de Lyon, France*

ABSTRACT

Cadenced wide-field imaging surveys in the upcoming decade will increase the number of identified $z < 0.3$ Type Ia supernovae (SNe Ia) from the hundreds to the hundreds of thousands. The increase in the number density of SNe Ia, in parallel with improvements in the standardization of their absolute magnitudes, now make them competitive probes of the growth of structure and hence of gravity. The peculiar velocity power spectrum is sensitive to γ, which captures the effect of gravity on the linear growth of structure through the relation $f = \Omega_M^\gamma$. In the next decade the peculiar velocities of SNe Ia in the local $z < 0.3$ Universe will provide a measure of γ down to 0.01 precision that can definitively distinguish between General Relativity and leading models of alternative gravity.

1.

In the late 1990's, Type Ia supernovae (SNe Ia) were used as distance probes to measure the homogeneous expansion history of the Universe. The remarkable discovery that the expansion is accelerating has called into question our basic understanding of the gravitational forces within the Universe. Either it is dominated by a "dark energy" that is gravitationally repulsive, or General Relativity is inadequate and needs to be replaced by a modified theory of gravity. It is only appropriate that in the upcoming decade, with their sheer numbers and improved distance precisions, SNe Ia will provide measurements of the *inhomogeneous* motions of structures in the Universe that will provide an unmatched test of whether dark energy or modified gravity is responsible for the accelerating expansion of the Universe.

In the next decade, SNe Ia will be used as peculiar-velocity probes to measure the influence of gravity on structure formation within the Universe. The peculiar velocity power spectrum is sensitive to the growth of structure as $P_{vv} \propto (fD)^2$, where D is the linear growth factor and $f \equiv \frac{d\ln D}{d\ln a}$ is the linear growth rate (Hui & Greene 2006; Davis et al. 2011).[1] The ΛCDM prediction for the $z = 0$ velocity power spectrum is shown in Figure 1. The growth of structure depends on gravity, indeed Linder & Cahn (2007) find that General Relativity, $f(R)$, and DGP gravities follow the relation $f \approx \Omega_M^\gamma$ with $\gamma = 0.55, 0.42, 0.68$ respectively. Adopting this parameterization to model gravity, peculiar velocity surveys are sensitive to $fD = \Omega_M^\gamma \exp\left(\int_a^1 \Omega_M^\gamma d\ln a\right)$, whose ΛCDM prediction is plotted in Figure 2 of Linder (2013).

Peculiar velocity surveys have already been used to measure fD, though not to a level where gravity models can be precisely distinguished. Adams & Blake (2017) use 6dFGS peculiar velocities using the Fundamental Plane method to get a 15% uncertainty in fD at $z \approx 0$ using density and velocity cross-correlations. The upcoming TAIPAN survey will obtain Fundamental Plane galaxies with densities of $n_g \sim 10^{-3} h^3\,\mathrm{Mpc}^{-3}$, and the WALLABY+WNSHS surveys

[1] To be precise, the peculiar velocity power spectrum also depends on the Hubble parameter as $P_{vv} \propto (HfD)^2$. A supernova survey measures luminosity distance fluctuations $\delta_{d_L} = (d_L - \bar{d}_L(z))/\bar{d}_L(z)$, where d_L is the observed distance and $\bar{d}_L(z)$ is the expected distance at the observed redshift z. To first order in peculiar velocity along the line of sight v, $\delta_{d_L} = v\left(1 - \frac{1}{H\bar{d}_L(z)}\right) \approx -\frac{v}{H\bar{d}_L(z)}$ at low redshift. The H-dependences of P_{vv} and the conversion from distances to velocities cancel, making peculiar velocity surveys sensitive to $(fD)^2$.

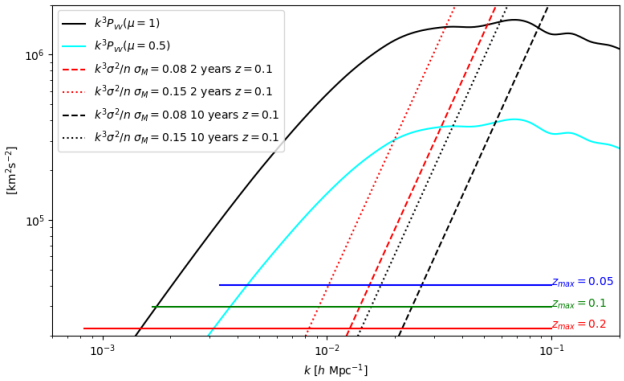

Figure 1. Volume-weighted velocity power spectrum $k^3P_{vv}(z=0)$ for $\mu=1, 0.5$ (solid black, cyan) as predicted for General Relativity in the linear regime. Volume-weighted peculiar velocity shot-noise $k^3\sigma^2/n$ at $z=0.1$, expected from 2- and 10-year (red, black) supernova densities, 0.08 and 0.15 mag (dashed, dotted) intrinsic magnitude dispersions. The bottom solid horizontal lines show the approximate range of k expected to be used in surveys with corresponding redshift depths z_{max}.

will obtain Tully-Fisher galaxies at densities $n_g \sim 2\times10^{-2} - 10^{-4}h^3\,\mathrm{Mpc}^{-3}$ from $z=0-0.1$. Covering 75% of the sky to a maximum depth of $z=0.1$, these surveys combined are projected to have 3% fD uncertainties (Howlett et al. 2017b). (For reference, DESI projects 10% precision of fD at $z>0.3$ redshifts using RSD alone.) Existing SN Ia samples have been used to test and ultimately find spatial correlations in peculiar velocities that may be attributed to the growth of structure (Abate & Lahav 2008; Johnson et al. 2014; Huterer et al. 2015, 2017).

Two advances in the upcoming decade will make SN Ia peculiar velocities more powerful. First, the precision of SN Ia distances can be improved. The commonly-used empirical 2-parameter SED model yields $\sigma_M \gtrsim 0.12$ mag absolute magnitude dispersion. However, SNe transmit more information than just the light-curve shape and single color used in current SN models. Recent studies indicate that with the right data, SNe absolute magnitudes can be calibrated to $\sigma_M \lesssim 0.08$ mag (see e.g. Barone-Nugent et al. 2012; Fakhouri et al. 2015). Though not yet established, it is anticipated that such a reduction in intrinsic dispersion comes with a reduction in the magnitude bias correlated with host-galaxy properties that is observed using current calibrations. One such SN is worth $\gtrsim 25$ galaxies with 0.4 mag absolute magnitude uncertainty. Secondly, in the upcoming decade cadenced wide-field imaging surveys such as ZTF and LSST will increase the number of identified $z<0.3$ Type Ia supernovae (SNe Ia) from the hundreds to the hundreds of thousands, over the course of 10-years, LSST will find $\sim 150,000$ $z<0.2$, $\sim 520,000$ $z<0.3$ SNe Ia for which good light curves can be measured, corresponding to a number density of $n\sim 5\times10^{-4}h^3\,\mathrm{Mpc}^{-3}$. This sample has comparable number density and more galaxies at deeper redshifts than projected by WALLABY and TAIPAN.

Given these two advances, over the course of a decade an LSST SN survey can produce interesting fD measurements in several redshift bins. Howlett et al. (2017a) find 4–14% uncertainties in fD in 0.05 redshift bins from $z=0$ to 0.3, where at $0<z<0.2$ most of the signal comes from peculiar velocities and at higher redshifts RSD is more constraining.

Our scientific interest is in probing gravity so we here focus on γ rather than on fD. To illustrate the distinction, $\frac{d(\ln fD)}{d\gamma} = \ln\Omega + \int \Omega^\gamma \ln\Omega\, d\ln a \approx -1.68, -0.75, -0.37$ at $z=0, 0.5, 1.0$ respectively in ΛCDM; two surveys with the same fractional precision in fD will have different precision in γ, with the one at lower redshift providing the tighter constraint. We project uncertainties in γ, σ_γ for a suite of idealized surveys using a Fisher matrix analysis similar to that of Howlett et al. (2017a,b). The Fisher information matrix is

$$F_{ij} = \frac{\Omega}{8\pi^2}\int_0^{r_{max}}\int_{k_{min}}^{k_{max}}\int_{-1}^{1} r^2k^2\mathrm{Tr}\left[C^{-1}\frac{\partial C}{\partial\lambda_i}C^{-1}\frac{\partial C}{\partial\lambda_j}\right]d\mu\,dk\,dr \tag{1}$$

where

$$C(k,\mu) = \begin{bmatrix} P_{\delta\delta}(k,\mu)+\frac{1}{n} & P_{v\delta}(k,\mu) \\ P_{v\delta}(k,\mu) & P_{vv}(k,\mu)+\frac{\sigma^2}{n}\end{bmatrix} \tag{2}$$

and the two parameters considered are $\lambda\in\{\gamma, bD\}$. The parameter dependence enters through $(fD)(\gamma)$ in the relations $P_{vv}\propto(fD\mu)^2$, the SN Ia host-galaxy overdensity power spectrum $P_{\delta\delta}\propto(bD+fD\mu^2)^2$, and the galaxy-velocity cross-correlation $P_{vg}\propto(bD+fD\mu^2)fD$, where b is the galaxy bias and μ is the cosine of the angle between the k-mode

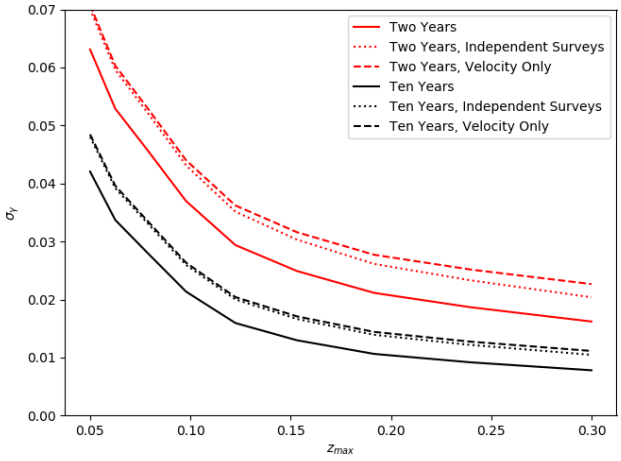

Figure 2. The projected uncertainty in γ achieved by two- (red) and ten-year (black) surveys of varying depth z_{max}. For each survey uncertainties are based on three types of analyses, one that only uses peculiar velocities (dashed), one that uses both overdensities (RSD) and peculiar velocities independently (dotted), and one that uses both RSD, peculiar velocities, and their cross-correlation (solid).

and the line of sight. While the bD term does contain information on γ, it is not used for making constraints. The uncertainty in γ is $\sigma_\gamma = \sqrt{(F^{-1})_{\gamma\gamma}}$. Non-GR models may also predict a change in the scale-dependence of the growth or non-constant γ, such observations provide additional leverage in probing gravity but are not considered here.

The uncertainty σ_γ of a survey depends on its solid angle Ω, depth r_{max} (or z_{max}), duration t through $n = \epsilon r t$ where r is the observer-frame SN Ia rate and ϵ is the sample-selection efficiency, and the intrinsic SN Ia magnitude dispersion through $\sigma \approx (\frac{5}{\ln 10}\frac{1+z}{z})^{-1}\sigma_M$. An analysis in which the RSD and velocity surveys are treated independently is achieved by setting the off-diagonal elements of C to zero.

We consider peculiar velocity surveys for a range of redshift depths z_{max} for survey durations of $t = 2$ and 10 years. The other survey parameters $\Omega = 3\pi$, $\epsilon = 0.65$, $\sigma_M = 0.08$ mag are fixed. The k-limits are taken to be $k_{min} = (2r_{max})^{-1}$ and $k_{max} = 0.1\ h\,\mathrm{Mpc}^{-1}$. The sample-selection efficiency ϵ is redshift-independent, i.e. the native redshift distribution is not sculpted. The input bias of SN Ia host galaxies is set as $b = 1.2$.

All the surveys considered can provide meaning tests of gravity. The projected uncertainty in γ achieved by the suite of surveys are shown in Figure 2. For each survey uncertainties are based on three types of analyses, one that only uses peculiar velocities, one that uses both overdensities (RSD) and peculiar velocities independently, and one that uses both RSD, peculiar velocities, and their cross-correlation. The short and shallow, 2-year, $z_{max} = 0.1$ survey has $\sigma_\gamma \sim 0.038$, which can distinguish between General Relativity, $f(R)$, and DGP gravities at the 2σ level. The 10-year survey performance asymptotes at $z_{max} \sim 0.2$ at a precision of $\sigma_\gamma \sim 0.01$. The figure also reveals an interesting interplay between RSD and velocity measurements. Peculiar velocities alone can account for much of the probative power of the surveys. RSD alone do not provide significant constraints. However, considering RSD and velocity cross-correlations decreases σ_γ by factors of ~ 0.8. There are important k-modes that are sample variance limited either in overdensity and/or peculiar velocity who benefit from the noise suppression engendered by cross-correlations.

Survey performance is examined in more detail by considering how σ_γ (using RSD, peculiar velocities, and their cross-correlations) changes with respect to the survey parameters Ω, z_{max}, t, and σ_M, and also with respect to differential redshift bins within a given survey.

Solid Angle Ω: The Fisher Matrix F is proportional to the survey solid angle Ω so $\sigma_\gamma \propto \sqrt{\Omega}$.

Differential Redshift Bin z: Certain redshifts constrain γ more strongly than others. If at a given moment of a survey we had a set of SNe Ia from which to choose, it turns out the one with the lowest redshift would be preferred. This is demonstrated to be the case at the end of both 2- and 10-year surveys and $z_{max} = 0.2$. Figure 3 shows $|\partial\sigma_\gamma/\partial z|$, which for both surveys monotonically decreases from $z = 0.01$ out to $z = 0.2$. If we had to sculpt the distribution (say due to limited follow-up resources), the preference would be to cut out the

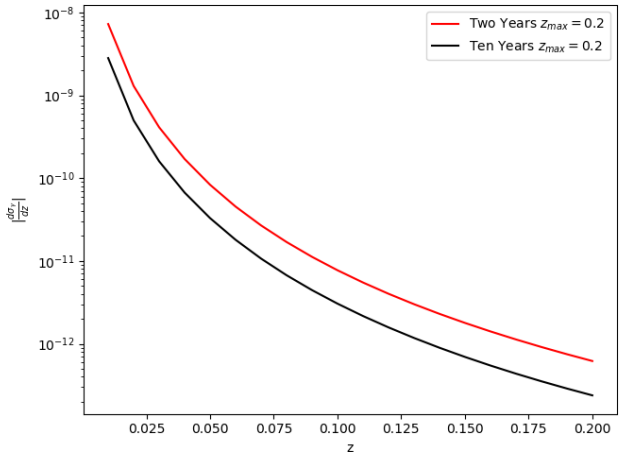

Figure 3. $|\partial\sigma_\gamma/\partial z|$ after two and ten years for a survy with limiting depth $z_{max} = 0.2$.

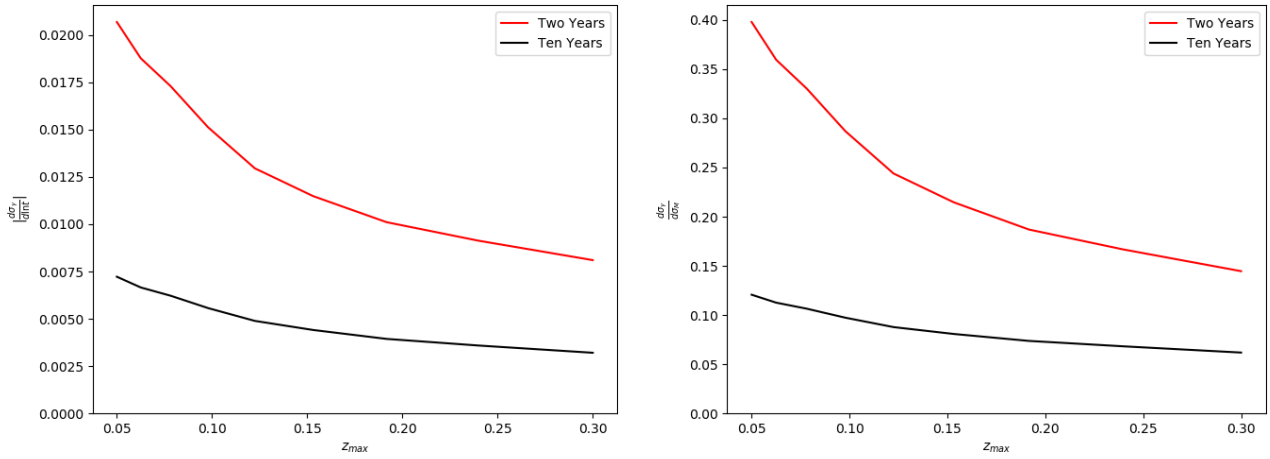

Figure 4. Left: $|\partial\sigma_\gamma/\partial \ln t|$ and Right: $\partial\sigma_\gamma/\partial\sigma_M$ as a function of z_{max} for two- and ten-year surveys.

highest redshift bins resulting in a decreased z_{max}. The optimal redshift distribution is thus the unsculpted SN-discovery distribution truncated by z_{max}.

Redshift Depth z_{max}: Increasing the survey redshift depth increases the γ precision. The differential improvement in σ_γ plateaus at $z_{max} \sim 0.2$ as seen in Figure 2.

Survey duration t; Intrinsic Magnitude Dispersion σ_M: Increasing the survey duration to increase the number density improves constraints. The benefit is stronger for shallow compared to deep surveys, and the strength of the benefit drops significantly over the course of 10 years. These trends are seen in the left panel of Figure 4, which plots $|\partial\sigma_\gamma/\partial \ln t|$ as a function of z_{max} for two- and ten-year surveys, and reflect those k-modes that do not benefit more data because they are sample-variance limited, either because they are at low k for shallow surveys or have already been saturated over the course of the survey. Like survey duration, intrinsic magnitude dispersion is related to survey performance through the shot noise and thus has similar relationships with σ_γ. This is evident in the plot of $\partial\sigma_\gamma/\partial\sigma_M$ shown in the right panel of Figure 4. The improvement between $\sigma_M = 0.08$ and 0.15 mag dispersions is equivalent to a factor of 3.52 in number density, or equivalently in survey duration.

From the above calculations, we find empirically that shot noise is important since higher number densities and lower intrinsic magnitude dispersion significantly reduce γ uncertainty, but that sample variance is also relevant by the end of a ten-year survey. Survey design is aided by understanding the circumstances in which the surveys become

sample variance limited. The rest-frame volumetric SN Ia rate is $7.84 \times 10^{-5} h^3\,\mathrm{Mpc}^{-3}\,\mathrm{yr}^{-1}$; after a few years the RSD measurement is sample variance limited. The contributions of P_{vv} and σ^2/n at $z = 0.1$ for $\sigma_M = 0.08, 0.15$ mag with number densities from 2- and 10-year surveys can be compared using Figure 1. For all of these survey scenarios, sample variance and shot-noise equality occurs at a k within the range that carries the most signal. However, the ten-year surveys do reach the sample variance limit for $k_{max} < 0.2\ h\,\mathrm{Mpc}^{-1}$.

1.1. *Designing an SN Ia Peculiar Velocity Survey*

There are different options to consider in the design of a SN Ia peculiar velocity survey, though at this point it is difficult to assess which is optimal or most cost effective. While there are a variety of recently identified indicators of SN Ia diversity that improve upon the 2-parameter model (SALT2) currently used to determine distances, there is not yet an umbrella model that simultaneously captures all indicators, their correlations, and characterizes the model residuals. Here we make several general conclusions based upon the above findings, while noting that constructing such a model is a parallel endeavor that will benefit peculiar-velocity and other SN Ia science.

- Spectroscopic transient classification: SNe Ia are defined through the absence of Hydrogen and the presence of the 6150 Å Silicon P-Cygni feature. The intrinsic magnitude dispersion depends on the purity of the sample. Conservatively, we consider a pure SN Ia sample obtained through spectroscopic classification; the requisite follow-up resources needed for complete $z < 0.3$ coverage is conceivable. The feasibility of using photometric classification is an important subject of research that can have implications for survey planning, particularly in extending the redshift range.

- Spectroscopic redshifts: Peculiar velocities are extracted directly from redshift measurements. Redshift uncertainties of $> 0.5\%$ contribute significantly to the error budget. We thus conclude that there is the need for spectroscopic $R > 200$ host-galaxy redshifts. In most cases this redshift will be available in the classification spectrum. Planned bright-galaxy redshift surveys can also observe a significant fraction of nearby SN hosts.

- Role of LSST: LSST can be taken to be a SN Ia discovery and distance machine, or a discovery machine only. LSST is expected to discover all $z < 0.3$ SNe Ia before maximum light in its active Wide Fast Deep (WFD) survey area. The nominal cadence produces sparse per-band light curves, which limits the intrinsic magnitude dispersion possible with LSST data alone to $\sigma_M \approx 0.15$ mag. The wide-field of LSST is well suited for discoveries over a larger area of sky, but does not provide significant multiplex advantage for the low surface-density of active $z < 0.3$ SNe Ia. LSST is suited for maximizing Ω while other (cheaper) resources that supplement LSST photometry can improve σ_M. The ultimate WFD observing strategy determines how well σ_8 can be determined with LSST data alone, and the amount of external resources needed (if any) to reach a targeted σ_M.

  The baseline LSST survey covers 18,000 sq. deg, at $-75 \lesssim \delta \lesssim 15$ avoiding the Galactic plane. Larger solid-angle coverage beyond the LSST baseline benefits peculiar-velocity science. Complementary northern-hemisphere surveys and LSST-expanded or independent coverage of the southern equatorial pole could significantly increase the sky coverage with a corresponding decrease in the variance of γ.

- Follow-up resources to determine per-SN distances: Supplemental non-LSST follow-up data in the form of improved temporal light-curve sampling (accurate rise and decline times), expanded (UV, NIR) wavelength coverage, and spectral features can access high-fidelity SN Ia models with lower intrinsic magnitude dispersion and residual systematic bias. For example, infrared data (Barone-Nugent et al. 2012) or spectrophotometry at peak brightness (Fakhouri et al. 2015) are projected to give $\sigma_M \lesssim 0.08$ mag.

  Scientific leverage dictates that low-redshift sources are most valuable. This aligns with observational considerations, for which closer and hence brighter objects require more modest follow-up resources. Therefore, z_{max} depends on the follow-up program as the redshift where complete follow-up saturates resources.

  A follow-up survey with $z_{max} = 0.2$ would have $\sim 150,000$ targets over 10 years. These sources will be observed when brighter than $r \sim 20.5$ mag and so will be accessible to 2–4m-class telescopes.

A low-redshift supernova survey is insensitive to two important uncertainties associated with the SN Ia Hubble diagram. The measurement is relatively insensitive to absolute color calibration, due to the limited range of *observer* wavelengths used to standardize restframe distance moduli. Depending on which cameras are used to derive distances,

instrumental (rather than absolute) calibration may be sufficient. Progenitor population is not expected to evolve significantly in the $0.01 < z < 0.2$ Universe.

2. CONCLUSIONS

SNe Ia are already powerful probes of the homogeneous cosmological expansion of the Universe. In the next decade. high-cadence, wide-field imaging surveys, together with improved precision in their distance determinations, will make SNe Ia powerful probes of the gravity induced-motion caused by the inhomogeneous Universe. SNe Ia peculiar velocities at $z < 0.3$ will measure $f\sigma_8$ significantly better than galaxy surveys, at lower redshifts that provide better leverage to test gravity models. While imaging surveys will provide a steady stream of SNe Ia, a coordinated plan of follow-up is required to take advantage of their probative power. The resources necessary to follow hundreds of thousands of SNe depend on specific follow-up choices, and access to those resources will define the redshift limits of the survey. Fortunately, the lowest-redshift, and hence brightest, supernovae are of the highest interest, so that a modest suite of ~ 5 2–4m telescopes should be capable of providing leading measurements of $f\sigma_8$ at $z \sim 0.1$.

An important survey parameter that is not considered is cost.

Effect of 10-years.

We are interested in

$$F_{00,\alpha}^{-1} = \frac{F_{11,\alpha}}{F_{00}F_{11} - F_{01}^2} - \frac{F_{11}}{(F_{00}F_{11} - F_{01}^2)^2} \left(F_{00,\alpha}F_{11} + F_{00}F_{11,\alpha} - 2F_{01}F_{01,\alpha}\right).$$

$$F_{ij} = \frac{\Omega}{8\pi^2} \int_0^{r_{max}} \int_{k_{min}}^{k_{max}} \int_{-1}^{1} r^2 k^2 \mathrm{Tr}\left[C^{-1}\frac{\partial C}{\partial \lambda_i} C^{-1} \frac{\partial C}{\partial \lambda_j}\right] d\mu\, dk\, dr \tag{3}$$

$$F_{ij,z} = \frac{\Omega}{8\pi^2} \frac{dr}{dz} r^2 \int_{k_{min}}^{k_{max}} \int_{-1}^{1} k^2 \mathrm{Tr}\left[C^{-1}\frac{\partial C}{\partial \lambda_i} C^{-1} \frac{\partial C}{\partial \lambda_j}\right] d\mu\, dk$$

$$F_{ij,s} = \frac{\Omega}{8\pi^2} \int_0^{r_{max}} \int_{k_{min}}^{k_{max}} \int_{-1}^{1} r^2 k^2 \mathrm{Tr}\left[C_{,s}^{-1}\frac{\partial C}{\partial \lambda_i} C^{-1} \frac{\partial C}{\partial \lambda_j} + C^{-1}\frac{\partial C}{\partial \lambda_i} C_{,s}^{-1} \frac{\partial C}{\partial \lambda_j}\right] d\mu\, dk\, dr$$

$$C = \begin{bmatrix} P_{gg}(k,\mu) + \frac{1}{n} & P_{vg}(k,\mu) \\ P_{vg}(k,\mu) & P_{vv}(k,\mu) + \frac{\sigma^2}{n} \end{bmatrix}. \tag{4}$$

$$C_{,n}^{-1} = \frac{n^{-2}((P_{gg}(k,\mu) + \frac{1}{n})\sigma^2 + (P_{vv}(k,\mu) + \frac{\sigma^2}{n}))}{\left((P_{gg}(k,\mu) + \frac{1}{n})(P_{vv}(k,\mu) + \frac{\sigma^2}{n}) - P_{vg}(k,\mu)^2\right)^2} \tag{5}$$

$$\times \begin{bmatrix} P_{vv}(k,\mu) + \frac{\sigma^2}{n} & -P_{vg}(k,\mu) \\ -P_{vg}(k,\mu) & P_{gg}(k,\mu) + \frac{1}{n} \end{bmatrix} \tag{6}$$

$$- \frac{n^{-2}}{(P_{gg}(k,\mu) + \frac{1}{n})(P_{vv}(k,\mu) + \frac{\sigma^2}{n}) - P_{vg}(k,\mu)^2} \begin{bmatrix} \sigma^2 & 0 \\ 0 & 1 \end{bmatrix}. \tag{7}$$

$$C_{,\sigma_M}^{-1} = \frac{\ln 10}{5} \frac{z}{1+z} \frac{2\sigma}{n} \Big(\frac{1}{(P_{gg}(k,\mu) + \frac{1}{n})(P_{vv}(k,\mu) + \frac{\sigma^2}{n}) - P_{vg}(k,\mu)^2} \begin{bmatrix} 1 & 0 \\ 0 & 0 \end{bmatrix} \tag{8}$$

$$- \frac{(P_{gg}(k,\mu) + \frac{1}{n})}{\left((P_{gg}(k,\mu) + \frac{1}{n})(P_{vv}(k,\mu) + \frac{\sigma^2}{n}) - P_{vg}(k,\mu)^2\right)^2} \tag{9}$$

$$\times \begin{bmatrix} P_{vv}(k,\mu) + \frac{\sigma^2}{n} & -P_{vg}(k,\mu) \\ -P_{vg}(k,\mu) & P_{gg}(k,\mu) + \frac{1}{n} \end{bmatrix} \Big) \tag{10}$$

$$\tag{11}$$

REFERENCES

Abate, A., & Lahav, O. 2008, MNRAS, 389, L47, doi: 10.1111/j.1745-3933.2008.00519.x

Adams, C., & Blake, C. 2017, MNRAS, 471, 839, doi: 10.1093/mnras/stx1529

Barone-Nugent, R. L., Lidman, C., Wyithe, J. S. B., et al. 2012, MNRAS, 425, 1007, doi: 10.1111/j.1365-2966.2012.21412.x

Bhattacharya, S., Kosowsky, A., Newman, J. A., & Zentner, A. R. 2011, PhRvD, 83, 043004, doi: 10.1103/PhysRevD.83.043004

da Cunha, E., Hopkins, A. M., Colless, M., et al. 2017, Publications of the Astronomical Society of Australia, 34, e047, doi: 10.1017/pasa.2017.41

Davis, T. M., Hui, L., Frieman, J. A., et al. 2011, ApJ, 741, 67, doi: 10.1088/0004-637X/741/1/67

Fakhouri, H. K., Boone, K., Aldering, G., et al. 2015, ApJ, 815, 58, doi: 10.1088/0004-637X/815/1/58

Howlett, C., Robotham, A. S. G., Lagos, C. D. P., & Kim, A. G. 2017a, ApJ, 847, 128, doi: 10.3847/1538-4357/aa88c8

Howlett, C., Staveley-Smith, L., & Blake, C. 2017b, MNRAS, 464, 2517, doi: 10.1093/mnras/stw2466

Hui, L., & Greene, P. B. 2006, PRD, 73, 123526, doi: 10.1103/PhysRevD.73.123526

Huterer, D., Shafer, D. L., & Schmidt, F. 2015, JCAP, 12, 033, doi: 10.1088/1475-7516/2015/12/033

Huterer, D., Shafer, D. L., Scolnic, D. M., & Schmidt, F. 2017, JCAP, 5, 015, doi: 10.1088/1475-7516/2017/05/015

Johnson, A., Blake, C., Koda, J., et al. 2014, MNRAS, 444, 3926, doi: 10.1093/mnras/stu1615

Johnston, S., Taylor, R., Bailes, M., et al. 2008, Experimental Astronomy, 22, 151, doi: 10.1007/s10686-008-9124-7

Linder, E. V. 2013, Journal of Cosmology and Astroparticle Physics, 2013, 031

Linder, E. V., & Cahn, R. N. 2007, Astroparticle Physics, 28, 481, doi: 10.1016/j.astropartphys.2007.09.003

Masters, K. L., Springob, C. M., & Huchra, J. P. 2008, AJ, 135, 1738, doi: 10.1088/0004-6256/135/5/1738

Odderskov, I., & Hannestad, S. 2017, JCAP, 1, 060, doi: 10.1088/1475-7516/2017/01/060

Springob, C. M., Magoulas, C., Colless, M., et al. 2014, MNRAS, 445, 2677, doi: 10.1093/mnras/stu1743

Tully, R. B., Courtois, H. M., & Sorce, J. G. 2016, AJ, 152, 50, doi: 10.3847/0004-6256/152/2/50